The hydrodynamic costs of spination in zoea

Gabriel Ng[1]

[1] Bodega Marine Lab, University of California Davis, Davis, California 95616, United States

Abstract

The benefits of spines in zoea and other crustaceans have been documented in numerous studies as a form of anti-predatory behavior. This study examined the potential costs of having spines using three different methods. Drag forces on spines were calculated using hydrodynamic equations and compared between zoea models with long and short spines; clay models were used in corn syrup sinking rate experiments to measure drag coefficients; and zoea models were created in FreeCAD and ran through a shear simulation in MATLAB to examine their stabilities. The study found that the presence of spines increased the drag forces on the models both through calculations and through direct measurements in corn syrup. Moreover, the presence of spines made models more susceptible to tumbling under shear when the spines were flared. However, if long spines were held in typical positions, the zoea models were actually more stable than the short spined model. This study highlights some of the plausible costs associated with spines and further studies are needed to examine the relative importance between hydrodynamic costs in spines versus decreased risk in predation.

Introduction

Life as a planktonic larva is fraught with numerous hazards with mortality being a major component. Mortality rates have been shown to be a significant component of the population dynamics within planktonic larvae (Thorson 1950; Rumrill (1990); Vaughn and Allen 2010). Lack of suitable habitat, scarcity of food, and potential risk of offshore transport are just some of the examples in which larvae can fail to survive past their planktonic stage (Pineda et al. 2009). The effects of mortality within the larval stage can have major implications in the recruitment of juveniles and the population dynamics of adults (Eggleston and Armstrong 1995).

In addition to possible starvation and lack of suitable settling substrate, predation can play a substantial role to mortality rates in larvae. Although the planktonic life stage of many benthic marine invertebrates has been hypothesized to act as a spatial refuge for benthic predators (Strathmann et al. 2002), predation in the water column can still be significant with estimates ranging from 0% to 90% (Allen and McAllister 2007; Kerr et al. 2014; the tunicate one, Johnson and Shanks 2003) With such possible high predation rates, various taxa have evolved anti-predatory defenses in their larval form. Some lecithotrophic larvae of sponges and tunicates are chemically defended from predators (Lindquist and Hay 1996). Some zooplankton have behavioral defenses, and alter their swimming depth behavior in diel vertical migration to escape from visual predators (Lampert 1989; Gliwicz 1986) Various taxa of crustaceans have morphological defenses, such as spination (Morgan 1989; Riessen 2012; Bollache et al. 2006). These spines potentially prevent gape-limited predators from successfully consuming prey and can injure predators that attempt to feed on larvae with spines. (Morgan 1989).

Rhithropanopeus harrisii, the estuarine mud crab, is a species of crab found natively along the east coasts of North America (Forward 2009). Like most other brachyuran zoea, *R. harrisii* larvae possess numerous spines as zoea. However, *R. harrisii* is unique in that it also

possesses relatively long antennal spines that can be flared out when agitated (Morgan 1989). Morgan (1989) demonstrated that the presence of spines in *R. harrisii* is effective in deterring predation by planktivorous fish. However, the relatively long protrusions in *R. harrisii* from both the antennal and rostral spines may increase the hydrodynamic costs of defense in spines. Other examples of anti-predatory adaptations, such as chemical defenses or behavioral changes are known to incur a significant cost to the prey (Nyland et al. 2013; Trussell et al. 2006). Studies conducted with *Daphnia pulex* and rotifers noted mixed effects when spines were induced in the presence of predators (Gilbert 2013; Riessen 2012). The long spines in *R. harrisii* could hypothetically reduce its swimming effectiveness, causing *R. harrisii* to either swim at a decreased speed compared to other species or for *R. harrisii* to increase its energy expenditure for a given speed. Hydrodynamic equations (Vogel 1994; Grünbaum 1995) show that the presence of any appendages should increase the drag on a moving body. This was demonstrated by Emlet (1983) where increased arm length in echnioplutei resulted in greater drag force.

The objective of this study is to characterize the potential swimming costs of spines in brachyuran zoeas. I hypothesize that the presence of spines increases drag forces on a zoea and that longer spines decrease the stability of a zoea in a turbulent environment. A variety of methods are used to test these hypotheses including calculating the net force on a zoea using equations, comparing those results with net force determined by using clay models, and simulating zoea of contrasting shapes in shear water using MATLAB.

Methods

To examine how spines influence the swimming characteristics of zoea, I first characterized the parameter space of the longest and shortest spine lengths in different species of crabs. Using keys created by Hernandoz et al. (2007), Dan et al. (2013), Rice et al. (2007), and

Souza et al. (2013), I measured the lengths of the carapace, dorsal spine, rostral spine, and abdomen of different species. In addition, lateral and antennal spines were measured if present in the zoea. Furthermore, the angles of the spines with respect to each other were recorded. After compiling the various measurements, I calculated the ratios of the spines and abdomens to the carapace length.

Forces on spines

From the equations laid out by Vogel (1994) and Grünbaum (1995), forces on three zoea morphologies could be determined. The first zoea morphology consisted of the longest ratios of spines and abdomen with respect to the carapace length; the second morphology consisted of the shortest ratios and the absence of lateral and rostral spines since some zoeas do not have either of those. The third morphology was a zoea with identical spine ratios as the second model; however, it occupied the same volume as the first zoea. Instead of having more spines, the third model had a larger diameter than the other two models. The first two zoea types represent the extreme range of possible morphologies, and the third zoea type accounts for the increase in drag force just due to an increase in volume and not necessarily the length and number of spines. It should also be noted that though porcellanid crabs were measured, they were not used in the models in order to constrain the possible spine ratios to just brachyuran crabs. Calculations were done in R, and the zoeas were scaled to be around the size of a first instar. I simplified the morphology of the zoeas so that the ceaphalothorax was treated as a sphere, and the abdomen and spines were treated as cylindrical rods. The first two zoeas have a diameter of 0.04 mm, and the sizes of their appendages were calculated from their respective ratios. The third zoea has a diameter of 0.05 mm.

The equation used to calculate the force on a body comes from Vogel (1994).

97 $$F = 6\pi\mu a U \qquad 1)$$

98 where F is the drag force on the sphere, mu is the dynamic viscosity of water, a is the radius of
99 the sphere, and U is the velocity of the sphere.

100 The drag force on a cylinder was calculated using the equations in Grünbaum (1995)

101 $$F_n = K_n L U_n \qquad 2)$$

102 $$F_t = K_t L U_t \qquad 3)$$

103 F_n represents the normal drag force on the cylinder, U_n is the normal component of the velocity,
104 L is the length of the cylinder, and K_n is the normal resistant coefficient. F_t, U_t, and K_t represent
105 the tangential component of drag force, velocity, and resistant coefficient respectively. The
106 resistant coefficients were calculated using the following equations in Grünbaum (1995)

107 $$K_n = \frac{8\pi\mu}{2\log\left(\frac{L}{r}\right)+1} \qquad 4)$$

108 $$K_n = \frac{8\pi\mu}{2\left(2\log\left(\frac{L}{r}\right)+1\right)} \qquad 5)$$

109 where r represents the radius of the cylinder and log represents the natural log.

110 Forces on the models were calculated with two velocity vectors. Jacoby (1982) measured
111 the swimming rate of the first instar of *Metacarcinus magister* to be around 0.95 cm/s. For the
112 calculations, I varied the estimated velocity in two different directions: one tangent to the rostral
113 and dorsal spines and one tangent to the abdomen. Sulkin (1984) found zoea to swim with their
114 dorsal spines 30 degrees but personal correspondence noted that zoea swim with their abdomen
115 tangent to the flow. By calculating the forces on the three models under the two velocity vectors,
116 it provides a possible range of forces zoeas experience as they orient themselves.

117 Sinking speed

In addition to calculating the drag forces on the zoeas, I compared sinking speeds of zoea models in corn syrup. For this experiment, I used similar methods laid out by Morgan (1989). Morgan (1989) recorded the sinking rates of *Rhithropanopeus harrisii* zoea with their spines clipped or intact; furthermore, he also examined *R. harrisii* zoea with their antennal spines flared out nearly orthogonal to the rostral spine. Using a clay ball of 10mm in diameter and appendages scaled to the body, I created three models of *R. harrisii*: one with spines in the normal orientation, one with spines in the flared orientation, and one without spines. Because the models with spines were heavier than the one without, a fourth model without spines was created with a similar weight to the spined models of 3.0g.

Sinking speeds were measured in a four-liter jar of 0.157m in diameter filled with corn syrup. Models were placed in the center of the jar with their rostral and dorsal spines horizontal and allowed to sink for several centimeters before measurements were recorded to diminish wall effects. Trials ended after 0.116 meters to also decrease the effects from the bottom of the jar. Each treatment was repeated 10 times. The drag coefficients were calculated using the equation

$$C_d = \frac{F}{\mu UL} \qquad 6)$$

Here, L is the characteristic length of the diameter of the sphere in order to compare how drag changes across different morphologies.

Simulated models in a current

To examine how spines influence stability, I first created virtual models of zoea in FreeCAD. The three models used in this experiment were the large ratio model, the small ratio model, and a flared large ratio model with antennal spines perpendicular to the rostral spine. Once created, the models were imported into MATLAB and subjected to a shear flow model created by Daniel Grünbaum (person correspondence). The shear forces were programmed to

flow horizontally with a vertical gradient as the zoea sank vertically. The output from the model illustrated the position of the zoea over time and all models reached an equilibrium position in no shear conditions. Shear was increased for all models until they fail to reach an equilibrium position and continued to tumble.

Results

Measuring the parameter space of spines in zoea

Table 1 presents the measured ratios of the respective spines or abdomen with respect to the carapace length (CL). The longest ratio zoea model used dorsal, rostral, abominal, and annetnal ratios from *R. harrisii* and lateral ratios from *Cancer antennarius*. The shortest ratio models used *Uca thayeri* for the dorsal ratio, *Portunus trituberculatus* for the abdominal ratio, and *Sesarma rectum* for the rostral ratio.

Forces on spines:

Table 2 depicts the forces on each component of the zoeas along with the cumulative forces on the model, making the assumption that forces are additive. By comparing the ratios of forces from the long spined model and the short spined, the long spined zoea experienced a force of 2.8x to 3.15x greater than the short spined zoea, depending on the orientation of the water current. When compared to the model with the same volume but short spines, the long spined model still experienced a force 2.27x to 2.55x greater, depending on the water current direction. Zoeas swimming with their rostral and dorsal spines orthogonal to the water current experience slightly more force than those swimming with their dorsal and rostral spines tangent to the water current. Table 3 shows the calculated drag coefficients on the models based on the calculated drag force, a fixed velocity of 0.95 cm/s, and a fixed characteristic length of the dorsal to the rostral spine of the shortest ratio model.

Sinking speeds

Figure 1 shows the sinking speeds of four different *R. harrisii* models in corn syrup. The model with flared spines sank the slowest, followed by one with long spines, then the despined model with the same carapace length as the other models, and finally, the model with no spines but with the same weight as the models with spines. A one way ANOVA followed by a TukeyHSD test determined that all four models had significantly different sinking rates ($p = 2.2e-16$). Table 4 shows the calculated drag coefficients based on the net force on the clay models, their average sinking velocities, and a fixed characteristic length of the diameter of the sphere. As expected, the drag coefficient is largest for the flared spined model with the smallest despined model having the smallest drag coefficient.

Simulated models in a current

The MATLAB simulation examined how morphology of zoea models affected their stability. Table 5 summarizes the shear force at which a model becomes unstable and will continue to rotate, never reaching an equilibrium position. The model with long spines flared out was the least stable model followed by the model with short spines. The model with long spines in a normal orientation had the most stable configuration, stabilizing itself at shear of up to $3.8s^{-}$, while the model with flared spines became unstable at shear of $2s^{-}$.

Discussion

Tradeoffs are ubiquitous in many adaptations. Whether it is symbiosis or spination, there are often costs to an adaptation, which can also vary depending on the environmental conditions (Bruno et al. 2003). In the case of spines on zoeas, I have shown that spines do incur a cost on the hydrodynamic properties of the larvae. Not only do spines increase the drag coefficients on a larval body, which was demonstrated by both calculations and measurements of sinking

187 velocities, but under certain orientations, spines also cause zoea to be less stable under shear
188 flow. The models also illustrate that it is the morphology of the spines and not just the increased
189 in volume that is causing changes in hydrodynamic properties. Models without spines but the
190 same weight as those with spines actually sank the fastest in corn syrup (Fig 1); similarly,
191 models with short spines but the same volume as models with long spines still experienced less
192 force on the body than models with long spines (Table 2).
193 Although the calculated drag coefficients of the sinking experiment and the force
194 calculations are not identical, the relative drag coefficients on the models are similar within both
195 experiments. The discrepancies between the two experiments can be explained by the
196 assumptions made in the calculations. By summing up the forces on the individual appendages, I
197 assumed that the spines do not interact with each other when producing drag. If this assumption
198 were violated, it would explain the differences in drag coefficients when calculating using a
199 model versus measuring the drag coefficient from an actual clay model.
200 The simulation experiment hints at a possible further benefit to long spines. Under high
201 shear conditions, the model with long spine actually had a higher stability than the on with short
202 spines. Although long spined models were the least stable when flared, Morgan (1989) noted that
203 flaring only occurred when zoeas were stressed. Under normal conditions, it is possible that the
204 spines act as a weather vane, and not only decrease predation risk but also stabilize zoeas.
205 Furthermore, while flared spines increase drag in zoeas, the associated decrease in sinking
206 velocity could potentially be beneficial in certain conditions.
207 Actual costs to zoea
208 Although this study has quantified the effects of having long spines in zoeas, it is still a
209 complicated process to measure the exact costs to them. A bioenergetics model of zoeas is

210 required to account for how a two to three times increased in drag will impact the energy budget
211 of a zoea. Some species of decapod larvae are lecithotrophic (Abrunhosa et al. 2008); if
212 lecithotrophic larvae only have a finite amount of energy reserves to develop and metamorphose,
213 they are unable to supplant the energy lost to increased drag with higher feeding rates.
214 Furthermore, a common currency is required to translate between swimming costs and costs of
215 predation risks. Morgan (1989) has calculated the decrease in predation risk associated with long
216 spines; however, the benefits will have to be converted into some common unit, such as survival
217 or fitness, to directly compare the cost of increased energy expenditure due to larger drag forces.
218 A similar method can be applied to the increase in stability due to long spines. While one can
219 suppose that a more stable morphology is beneficial to a zoea, the advantages of a more stable
220 morph will have to be converted into increase in fitness in order to analyze if the cost of
221 increased drag outweighs the benefits of increased stability and decreased predation.
222 The life-dinner principle (Dawkins and Krebs 1979) could provide some insight to the
223 relative costs and benefits, however. According to the hypothesis, in a predator-prey relationship,
224 prey will experience stronger selection to prevent predation events than a predator will have to
225 catch a prey. For the prey, being captured results in a loss of all future offspring, while failure to
226 catch one prey does not necessarily translate to instant mortality and loss of all fecundity for the
227 predator. Although this study only examined the costs to the prey, the life-dinner principle could
228 explain why having substantial costs in swimming characteristics might be beneficial since it
229 deters predation.
230 An alternative explanation for the presence spines is that zoeas with long spines swim
231 slower. Consequently, they do not incur an energetic cost even with higher drag coefficients.
232 Though this could make them more susceptible to predation events, zoeas with long spines are

already relatively protected from predators. Therefore, the potentially slower swimming speeds of long-spined zoeas might not have a significant cost to them. This explanation does not take into account the possible decrease in foraging as swimming speed slows (Abrunhosa et al. 2011).

While this study quantified how swimming properties change as spine lengths increase, there are still multiple ways of elaborating on this study. In all models, I made the assumption that a zoea can be modeled as a sphere for the cephalothorax and the spines as cylinders. Even though these simplified shapes cover most of the zoea morphospace, the swimming appendages, such as the maxillipeds are not modeled. Moreover, in the MATLAB simulations, the zoeas were modeled to be sinking at all times. The results provided do not take into account the swimming behavior of zoea or how they would orient themselves if they were not a passive particle. In addition, although I have modeled the antennal spines in two different and extreme orientations, it is possible that *R. harrisii* can orient its antennal spines in a more efficient manner.

Despite the possible limitations in this study, I have demonstrated there are possible costs to having long spines in zoea. While other studies have demonstrated their benefits (Morgan, 1989), cost of spination will have to be accounted for in assessing the possible adaptive value of various spine morphologies. Quantifying the tradeoffs associated with variations in morphological traits can potentially elucidate the presence or absence of morphology and behaviors in marine larvae, which can have further implications on the distribution and abundance of different brachyuran crab species.

References

Abrunhosa, F. A., Simith, D. J., Monteiro, J. R., Souza Junior, A. N. D., & Oliva, P. A. 2011. Development and functional morphology of the larval foregut of two brachyuran species from Northern Brazil. Anais da Academia Brasileira de Ciências, 83: 1269-1278.

Abrunhosa, F. A., Simith, D. J., Palmeira, C. A., & Arruda, D. C. 2008. Lecithotrophic behaviour in zoea and megalopa larvae of the ghost shrimp *Lepidophthalmus siriboia* Felder and Rodrigues, 1993 (Decapoda: Callianassidae). Anais da Academia Brasileira de Ciências, 80: 639-646.

Allen, J. D., & McAlister, J. S. 2007. Testing rates of planktonic versus benthic predation in the field. Journal of Experimental Marine Biology and Ecology, 347: 77-87.

Bollache, L., Kaldonski, N., Troussard, J. P., Lagrue, C., & Rigaud, T. 2006. Spines and behaviour as defences against fish predators in an invasive freshwater amphipod. Animal behaviour, 72: 627-633.

Bruno, J. F., Stachowicz, J. J., & Bertness, M. D. 2003. Inclusion of facilitation into ecological theory. Trends in Ecology & Evolution, 18: 119-125.

Dan, S., Kaneko, T., Takeshima, S., Ashidate, M., & Hamasaki, K. 2013. Variations in larval morphology and their relationships to survival during mass seed production by the swimming crab, *Portunus trituberculatus* (Brachyura, Portunidae). Aquaculture, 414: 109-118.

Dawkins, R., & Krebs, J. R. 1979. Arms races between and within species. Proceedings of the Royal Society of London. Series B. Biological Sciences, 205: 489-511.

Eggleston, D. B., & Armstrong, D. A. 1995. Pre-and post-settlement determinants of estuarine Dungeness crab recruitment. Ecological Monographs, 65: 193-216.

Emlet, R. B. 1983. Locomotion, drag, and the rigid skeleton of larval echinoderms. The Biological Bulletin, 164: 433-445.

Forward, R. B. 2009. Larval biology of the crab *Rhithropanopeus harrisii* (Gould): a synthesis. The Biological Bulletin, 216: 243-256.

Gilbert, J. J. 2013. The cost of predator-induced morphological defense in rotifers: experimental studies and synthesis. Journal of plankton research, 35: 461-472.

Gliwicz, M. Z.1986. Predation and the evolution of vertical migration in zooplankton. Nature, 320:746-748.

Grünbaum, D. 1995. A model of feeding currents in encrusting bryozoans shows interference between zooids within a colony. Journal of Theoretical Biology, 174: 409-425.

303 Hernández, G., Bolaños, J., Magán, I., & Graterol, K. 2007. Morfología de la primera zoea de los
304 cangrejos marinos *Petrolisthes haigae* y *P. nobilii* (Decapoda: Porcellanidae). Revista de
305 biología tropical, 55: 879-887.
306
307 Jacoby, C. A. 1982. Behavioral responses of the larvae of *Cancer magister* Dana (1852) to light
308 pressure, and gravity. Marine & Freshwater Behaviour & Phy, 8: 267-283.
309
310 Kerr, K. A., Cornejo, A., Guichard, F., & Collin, R. 2014. Planktonic predation risk varies with
311 prey life history stage and diurnal phase. Marine Ecology Progress Series, 503: 99-109.
312
313 Lampert, W. 1989. The adaptive significance of diel vertical migration of zooplankton.
314 Functional Ecology, 3: 21-27.
315
316 Lindquist, N., & Hay, M. E. 1996. Palatability and chemical defense of marine invertebrate
317 larvae. Ecological Monographs, 6: 431-450.
318
319 Morgan, S. G. 1989. Adaptive significance of spination in estuarine crab zoeae. Ecology, 70:
320 464-482.
321
322 Nylund, G. M., Enge, S., & Pavia, H. 2013. Costs and benefits of chemical defence in the red
323 alga *Bonnemaisonia hamifera*. PloS one, 8: e61291.
324
325 Pineda, J., Reyns, N. B., & Starczak, V. R. 2009. Complexity and simplification in
326 understanding recruitment in benthic populations. Population ecology, 51: 17-32.
327
328 Rice, A., & Tsukimura, B. 2007. A key to the identification of brachyuran zoeae of the San
329 Francisco Bay estuary. Journal of Crustacean Biology, 27: 74-79.
330
331 Riessen, H. P. 2012. Costs of predator-induced morphological defences in *Daphnia*. Freshwater
332 Biology, 57: 1422-1433.
333
334 Rumrill, S.S., 1990. Natural mortality of invertebrate larvae. Ophelia 32, 163-198.
335
336 Souza, A. S. D., Costa, R. M. D., & Abrunhosa, F. A. 2013. Comparative morphology of the first
337 zoea of twelve brachyuran species (Crustacea: Decapoda) from the Amazon region.
338 Zoologia (Curitiba), 30: 273-290.
339
340 Strathmann, R. R., Hughes, T. P., Kuris, A. M., Lindeman, K. C., Morgan, S. G., Pandolfi, J. M.,
341 & Warner, R. R. 2002. Evolution of local recruitment and its consequences for marine
342 populations. Bulletin of Marine Science, 70: 377-396.
343
344 Sulkin, S. D. 1984. Behavioral basis of depth regulation in the larvae of brachyuran crabs.
345 Marine ecology. Progress series, 15: 181-205.
346
347 Thorson, G. 1950. Reproductive and larval ecology of marine bottom invertebrates. Biological
348 Reviews, 25: 1-45.

Trussell, G. C., Ewanchuk, P. J., & Matassa, C. M. 2006. Habitat effects on the relative importance of trait-and density-mediated indirect interactions. Ecology Letters, 9: 1245-1252.

Vaughn, D., & Allen, J. D. 2010. The peril of the plankton. Integrative and Comparative Biology, 50: 552-570.

Vogel, S. 1981. Life in Moving Fluids. Boston, MA: Willard Grant Press.

360 Table 1. A summary of the different ratios of the spines and abdomen to the carapace length (CL)
361 for different species of zoea.
362

Species	Dorsal/CL	Rostral/CL	Lateral/CL	Abdomen/CL	Dorsal thickness/Cl
Cancer antennarius /gracilis	1.00	0.50	0.66	1.50	0.20
Cancer productus	1.20	0.80	0.33	2.00	0.18
Carcinus maenas	1.04	0.80	N/A	1.67	0.19
Eurytium limosum	1.20	1.13	N/A	1.87	0.17
Pachygrapsus crassipes	0.59	0.63	0.51	1.32	0.18
Petrolisthes haigae	1.15	3.06	N/A	0.99	0.10
Petrolisthes nobilii	0.89	2.93	N/A	0.59	0.07
Pinnotheridae	2.00	1.67	0.60	1.33	0.20
Portunus trituberculatus	0.37	0.54	N/A	1.01	0.17
Rhithropanopeus harrisii	1.40	2.86	0.37	2.05	0.14
Sesarma rectum	0.50	0.42	N/A	1.83	0.14
Uca rapax	0.50	0.47	N/A	1.52	0.15
Uca thayeri	0.38	0.56	N/A	1.73	0.14
Species	Rostral thickness/Cl	Lateral thickness/Cl	Abdm thickness/Cl	Antennal/Cl	Antennal thickness/Cl
Cancer antennarius /gracilis	0.22	0.12	0.24	N/A	N/A
Cancer productus	0.20	0.12	0.40	N/A	N/A
Carcinus maenas	0.09		0.25	N/A	N/A
Eurytium limosum	0.16		0.37	N/A	N/A
Pachygrapsus crassipes	0.14	0.10	0.40	N/A	N/A
Petrolisthes haigae	0.11		0.15	N/A	N/A
Petrolisthes nobilii	0.11		0.12	N/A	N/A
Pinnotheridae	0.16	0.18	0.33	N/A	N/A
Portunus trituberculatus	0.13		0.25	N/A	N/A
Rhithropanopeus harrisii	0.14	0.11	0.31	2.56	0.13
Sesarma rectum	0.10		0.22	N/A	N/A
Uca rapax	0.16		0.31	N/A	N/A
Uca thayeri	0.18		0.35	N/A	N/A

363
364

364 Table 2. A summary of the individual force components acting on the appendages in model with
365 the largest spine ratios, model with the smallest spine ratios and the same carapace length as the
366 large spined model, and a model with the smallest spine ratios and the same volume as the large-
367 spined model.

	Tangent to rostral and dorsal		
Force (N)	Largest ratio	Smallest ratio	Large volume but smallest ratio
Abdomen	4.08E-09	2.10E-09	2.60E-09
Dorsal spine	1.36E-09	5.33E-10	6.60E-10
Rostral spine	2.49E-09	4.82E-10	5.97E-10
Lateral spine	1.58E-09		
Lateral spine	1.58E-09		
Antennal spine	3.05E-09		
Antennal spine	3.05E-09		
Carapace length	4.68E-09	4.68E-09	5.79E-09
Total force (N)	2.19E-08	7.79E-09	9.65E-09
Ratio of large ratio to small	2.80		
Ratio of large ratio to large volume but small ratio	2.27		
	Tangent to abdomen		
Force (N)	Largest ratio	Smallest ratio	Large volume but smallest ratio
Abdomen	2.26E-09	1.16E-09	1.44E-09
Dorsal spine	2.45E-09	9.61E-10	1.19E-09
Rostral spine	4.50E-09	8.70E-10	1.08E-09
Lateral spine	1.52E-09		
Lateral spine	1.52E-09		
Antennal spine	3.63E-09		
Antennal spine	3.63E-09		
Carapace length	4.68E-09	4.68E-09	5.79E-09
Total force (N)	2.42E-08	7.67E-09	9.50E-09
Ratio of large ratio to small	3.15		
Ratio of large ratio to large volume but small ratio	2.55		

368

Table 3 shows the parameters calculated and measured to find the drag coefficients of the 3 different models in R. Drag coefficients were calculated for current velocity tangent to the rostral and dorsal spines and for current velocity tangent to the drag coefficient.

Tangent to rostral and dorsal spines	Largest ratio	Smallest ratio	Large volume but smallest ratio
Force on model (N)	2.19E-08	7.79E-09	9.65E-09
Velocity (m/s)	0.0095	0.0095	0.0095
Characteristic length (m)	6.37E-05	6.37E-05	6.37E-05
Drag coefficient	27.63	9.85	12.20
Tangent to abdomen	Largest ratio	Smallest ratio	Large volume but smallest ratio
Force on model (N)	2.42E-08	7.67E-09	9.50E-09
Velocity (m/s)	0.0095	0.0095	0.0095
Characteristic length (m)	7.17E-05	7.17E-05	7.17E-05
Drag coefficient	27.17	8.62	10.68

Table 4 summarizes the parameters and measurements needed to calculate the drag coefficients from the sinking rate experiments for the 4 different types of models.

	Despined	Normal	Flared	Despined
Weight (kg)	0.002	0.003	0.0031	0.003
Net force on models (N)	0.0029	0.0044	0.0046	0.0044
Velocity (m/s)	0.0018	0.0014	0.0011	0.0020
Characteristic length (diameter of sphere (m))	0.053	0.053	0.053	0.053
Drag coefficients	22.3	44.3	55.4	20.8

406

407 Table 5. A summary of the shear needed to cause unstable tumbling in the MATLAB simulation

408 for three different zoea models: a short zoea model with the shortest spine ratios, a long zoea

409 model with the longest spine ratios, and another long zoea model with the antennal spines flared.

	Shear force when tumbling begins (s^{-1})
Short zoea	3.6
Long zoea	2
Long flared zoea	3.8

410
411

Figure 1. Sinking velocity across the 4 different models. A despined model with the same sphere diameter as the flared and normal model, a despined heavy model with the same mass as the flared and normal model, a flared model with antennal spines perpendicular to the rostrum, and a normal model based off on the dimensions of *R. harrisii*. Stars indicate significant differences ($F = 244.1$, $n = 10$, $p = 2.2e\text{-}16$).

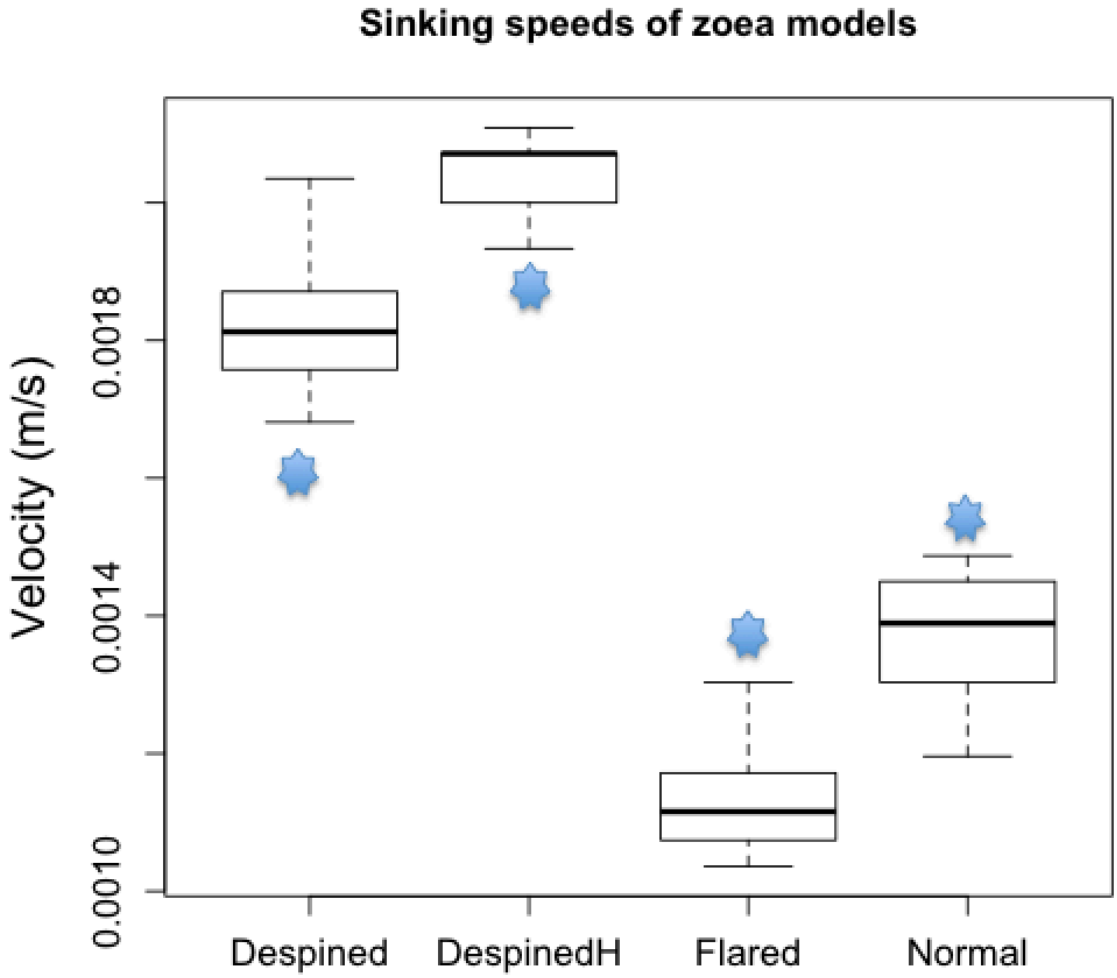
Sinking speeds of zoea models
Velocity (m/s)
0.0010
0.0014
0.0018
Despined
DespinedH
Flared
Normal

417

Appendices: R code to calculate forces on cylinders and spheres

```
#Parameters to input
# L = (0.0264)*1e-3 #magnitude of length of lateral in meters
    # L=(0.081860465e-3) #abdomen large
    # L=(0.055813953e-3) #dorsal large
    # L=(0.122222222e-3) #rostral large
    # L=(0.0264e-3)       #lateral large
    # L=(0.102325581e-3)  #antennal large

    # L=(0.040268456e-3) #abdomen small
    # L=(0.015e-3) #dorsal small
    # L=(0.016666667e-3) #rostral small

    # L=(0.049848926e-3) #abdomen small ratio but large volume
    # L=(0.018568725e-3) #dorsal small ratio but large volume
    L=(0.020631917e-3) #rostral small rostral but large volume

# e_tnon = c(-5,5.3,13.5) #non normalized direction of
 tangential vector of spine (x,y,z)
    # e_tnon = c(-33.6, 19.3,0) #abdomen
    # e_tnon = c(0, 19.4,   0) #dorsal
    e_tnon = c(0,   -45,    0) #rostral
    # e_tnon = c(-5,    5.3,    13.5) #lateral 1
    # e_tnon = c(-5,    5.3,    -13.5) #lateral 2
    # e_tnon = c(2, -38.1,  38.4) #antennal 1
    # e_tnon = c(2, -38.1,  -38.4) #antennal 2
# d=(0.0072)*1e-3 #diameter of dorsal in meters
    # d = (0.016e-3) #abdomen large
    # d=(0.007407407e-3) #dorsal large
    # d=(0.0088e-3) #rostral large
    # d=(0.0072e-3) #lateral large
    # d=(0.005302326e-3) #antennal large

    # d=(0.008888889e-3) #abdomen small
    # d=(0.0055e-3) #dorsal small
    # d=(0.003703704e-3) #rostral small

    # d=(0.011003689e-3) #abdomen small ratio but large volume
    # d=(0.006808533e-3) #dorsal small ratio but large volume
```

```
    d=(0.00458487e-3) #rostral small ratio but large volume

U=0.95/100 #speed of water current or speed of zoea swimming
 (m/s)
e_unon= c(0,-1,0) #non-normalized direction vector of current
 tangent to rostral and dorsal
 # e_unon=c(-33.6,  19.3,0) #velocity tangent to abdomen
mu= 1.307e-3 #dynamic viscosity of seawater at 10C (N*s/m2)

F.mag=function(L,e_tnon,d,U,e_unon,mu)
{
norm=sqrt(sum(e_tnon*e_tnon)) #normalizing the directional
 vector to                                  give a legnth of
 one (unit vector)
e_t = 1/norm*e_tnon #unit tangential vector
L_vector = L*e_t #Length vector
#L_vector and L are not actually used in the function

normeu=sqrt(sum(e_unon*e_unon))
e_u=e_unon/normeu #normalized direction vector of current
U_vector=U*e_u  #current vector

#finding the tangent component of velocity
U_tan=U*sum(e_u*e_t)*e_t
#finding the normal component of velocity
U_norm=U_vector-U_tan

r = d/2 #(radius of dorsal spines in meters)

Ktx=8*pi*mu/(2*(2*log(L/r)+1))
Knx=8*pi*mu/(2*log(L/r)+1)

Fnorm_vector1=U_norm[1]*L*Knx
Fnorm_vector2=U_norm[2]*L*Knx
Fnorm_vector3=U_norm[3]*L*Knx
Fnorm_vector=data.frame(Fnorm_vector1,Fnorm_vector2,Fnorm_vect
 or3)

```

```
495
496  Ftan_vector1=U_tan[1]*L*Ktx
497  Ftan_vector2=U_tan[2]*L*Ktx
498  Ftan_vector3=U_tan[3]*L*Ktx
499  Ftan_vector=data.frame(Ftan_vector1,Ftan_vector2,Ftan_vector3)
500
501  Ftotal_vector=Ftan_vector+Fnorm_vector
502  Ftotal_magnitudex=sqrt(rowSums(Ftotal_vector*Ftotal_vector))
503  test.dataframe=data.frame(L,Ktx,Knx,Fnorm_vector[1],Fnorm_vect
504   or[2],Fnorm_vector[3],Ftan_vector[1],Ftan_vector[2],Ftan_vect
505   or[3],Ftotal_magnitudex)
506  return(test.dataframe)
507  }
508  spine.force.mag=F.mag(L,e_tnon,d,U,e_unon,mu)
509  head(spine.force.mag)
510
511  #Sphere function
512  # length.sphere=0.04e-3
513  length.sphere=0.0495166e-3 #for large but small ratio
514  rad.sphere=length.sphere/2
515
516  F.sphere=function(y)
517  {   Force.sphere1=6*pi*mu*y*U_vector[1]
518   Force.sphere2=6*pi*mu*y*U_vector[2]
519   Force.sphere3=6*pi*mu*y*U_vector[3]
520   Force.sphere=data.frame(Force.sphere1,Force.sphere2,Force.sph
521   ere3)
522  Force.sphere.mag=sqrt(rowSums(Force.sphere*Force.sphere))
523  Function.dataframe=data.frame(y,Force.sphere1, Force.sphere2,
524   Force.sphere3,Force.sphere.mag)
525   return(Function.dataframe)}
526
527  sphere.force=F.sphere(rad.sphere)
528  sphere.force
529
530  #Calculating Re number
531  rho.water=1029 #kg/m3
532  rho.syrup=1380 #kg/m3
```

```
mu.syrup=1.3806 #Pa*s
speed= 0.95/100 #m/s
# L=(0.122222222+0.055813953+0.04)*1e-3 #m dorsal to rostral
 length for long zoea
# L=(0.015+0.016666667+0.04)*1e-3 #m dorsal to rostral length
 for short zoea
L=(0.018568725+0.020631917+0.0495166)*1e-3 #m dorsal to
 rostral length for short zoea
Re=rho.water*speed*L/mu

#1 DespinedH 0.002036567 a 35.9mm abdomen to body
#2 Despined  0.001819799 b 33.5mm abdomen to body
#3 Normal    0.001372152 c 44.7mm dorsal to rostral
#4 Flared    0.001133347 d 46.5mm dorsal to rostral
```